Assessing the near threshold cross section of the ^{17}O(n,α)^{14}C reaction by means of the Trojan horse method

G. L. Guardo, C. Spitaleri, L. Lamia, M. Gulino, M. La Cognata, X. Tang, R. deBoer, X. Fang, V. Goldberg, J. Mrazek, A. Mukhamedzhanov, M. Notani, R. G. Pizzone, G. G. Rapisarda, M. L. Sergi, and M. Wiescher

Phys. Rev. C **95**, 025807 — Published 21 February 2017

DOI: 10.1103/PhysRevC.95.025807

Assessing the near threshold cross section of the $^{17}O(n,\alpha)^{14}C$ reaction by means of the Trojan Horse Method

G.L. Guardo[1], C. Spitaleri[1,2], L. Lamia[2], M. Gulino[1,3], M. La Cognata[1], X. Tang[4], R. deBoer [4], X. Fang[4], V. Goldberg[6], J. Mrazek[5], A. Mukhamedzhanov[6], M. Notani[4], R.G. Pizzone[1], G.G. Rapisarda[1], M.L. Sergi[1], M. Wiescher[4]

[1] *INFN, Laboratori Nazionali del Sud, Catania, Italy*

[2] *Dipartimento di Fisica e Astronomia, Universitá degli studi di Catania, Catania, Italy*

[3] *University of Enna "Kore", Enna, Italy*

[4] *Department of Physics, Joint Institute for Nuclear Astrophysics, University of Notre Dame, Indiana, USA*

[5] *Nuclear Physics Institute of ASCR, Rez, Czech Republic*

[6] *Cyclotron Institute, Texas A&M University, College Station, TX 77843, USA*

(Dated: January 26, 2017)

The study of the $^{17}O(n,\alpha)^{14}C$ reaction has been performed by means of the Trojan Horse Method (THM) applied to the quasi-free $^{2}H(^{17}O,\alpha^{14}C)^{1}H$ reaction induced at a beam energy of 43.5 MeV. The THM allowed us to study the 8121 keV $^{18}O^{*}$ resonant level, for which the previous THM investigation pointed out the ability of the method to overcome the centrifugal barrier suppression effects in the entrance channel. Here, in view of the developments of the method for resonant reactions, the detailed analysis of the performed experiment will be discussed, focusing on the extraction of the 8121 keV resonance strength for which no information are present in scientific literature. Moreover, the experimental results clearly show the excitation of the subthreshold level centered at -6 keV in the center-of-mass system, which is fundamental to determine the $^{17}O(n,\alpha)^{14}C$ reaction rate of astrophysical interest. Finally, a new recommended reaction rate is presented for future astrophysical application.

I. INTRODUCTION

Nuclear reactions producing or absorbing neutrons are of key interest in several domains of both nuclear physics and astrophysics. The present work focuses on the recent study of the $^{17}O(n,\alpha)^{14}C$ reaction, for which at least two important areas of interest can be identified. In stellar nucleosynthesis of massive stars (with initial masses $M>8M_{\odot}$), this process can be considered as a "neutron-poison" for the so called weak *s*-process since it has the net effect of reducing the total neutron flux [4]. In such stars, the main neutron sources are the $^{13}C(\alpha,n)^{16}O$ and $^{22}Ne(\alpha,n)^{25}Mg$ reactions and the ignition of the $^{16}O(n,\gamma)^{17}O$ reaction is expected due to the presence of oxygen from CNO cycling [5]. The produced ^{17}O can experience both (α,n) or (n,α) reactions; the $^{17}O(\alpha,n)^{20}Ne$ reaction represents a recycle channel for the neutron flux while the $^{17}O(n,\alpha)^{14}C$ reaction is a neutron absorbing reaction. Therefore, the knowledge of the ratio between the cross section of these reactions is important to determine the overall neutron flux available for the *s*-process.

In addition, in applied nuclear physics, it is among the key reactions producing the radioactive ^{14}C isotope ($T_{1/2}$=5730 years) in nuclear reactors, together with the $^{14}N(n,p)^{14}C$ reaction. Since both ^{17}O and ^{14}N can be present as impurities in the materials constituting the reactor structure and fuel, neutron induced reactions can be easily ignited and the produced ^{14}C released in the atmosphere as carbon dioxide, thus constituting a dangerous possible contaminant for the life-cycle, being carcinogenic [1].

The reasons given above justify the studies of the $^{17}O(n,\alpha)^{14}C$ reaction in the energy window of interest for applied physics and astrophysics, namely from thermal up to ∼400 keV neutron energies. In this range, the intermediate compound ^{18}O nucleus exhibits four different states that contribute to the total cross section. The 8039 keV level ($J^{\pi}=1^{-}$) lies -6 keV below the neutron threshold, while the states at 8121 keV ($J^{\pi}=5^{-}$), 8224 keV ($J^{\pi}=2^{+}$), and 8289 keV ($J^{\pi}=3^{-}$) lead to three resonances at ∼75 keV, ∼178 keV, and ∼244 keV, respectively, in the $^{17}O(n,\alpha)^{14}C$ excitation function [6–8].

The $^{17}O(n,\alpha)^{14}C$ process has been extensively studied in the past by different authors by means of direct experiments and by applying the detailed balance principle to the inverse reaction. A summary of the results is displayed in Fig.1. The work of Sanders *et al.* [9] reports on the $^{17}O(n,\alpha)^{14}C$ investigation by means of the inverse experiment $^{14}C(\alpha,n)^{17}O$ and the corresponding results are shown as black points. These data are superimposed on the data of Koehler & Graff [10], displayed as red symbols and obtained by using a neutron beam on oxygen targets (anodized niobium Nb_2O_5). As for the data of [9], a line is given for easing the visualization. For the two sets of data a clear disagreement appears in correspondence of

the observed resonances, thus requiring further investigations. The work of Schatz *et al.* [11] is mainly focused on extracting the reaction rate by using their own measurement (shown as blue open symbols in Fig.1), for neutron energies between ∼100 keV and ∼220 keV, coupled with the measurements of [9] (at higher energies) and [10] (at lower energies). The most recent ^{17}O(n,α)^{14}C cross section measurement was performed by Wagemans *et al.* [8] and the corresponding data are shown as open triangles in Fig.1, clearly showing the contribution of the two resonances at neutron energies of about ∼180 keV and ∼250 keV. The disagreement among the different data sets shown here clearly causes a difference in the calculated total reaction rate, evaluated in the work of Wagemans *et al.* [8] to be of about a factor 2.5-3 in the astrophysically relevant energy region.

The previously mentioned direct measurement of Wagemans *et al.* [8] has been recently corroborated by the indirect ^{17}O(n,α)^{14}C investigation performed via the Trojan Horse Method (THM) [12–16], published in Gulino *et al.* [17]. The THM study allowed us to cover the energy region of interest for astrophysics and to assess the contribution of the two already known resonant levels observed by Wagemans *et al.* [8]. In addition, the THM measurement allowed us to determine the influence of the 8121 keV f-wave resonant level.

This work is mainly focused on the extraction of spectroscopic information about the 8121 keV level, with particular emphasis on the determination of its strength. Indeed, since it is a narrow resonance, resonance strength is the key parameter for calculating the reaction rate, besides the resonance energy. The second goal is the calculation of the precise contribution of the -6 keV resonance to the total reaction rate, expecially with respect to the 1/v contribute that dominate the low energy astrophysical region. The detailed analysis of the experiment will be discussed, focusing on the different steps of a typical THM analysis. Finally, we will discuss a recommended reaction rate, calculated merging the best literature results with ours.

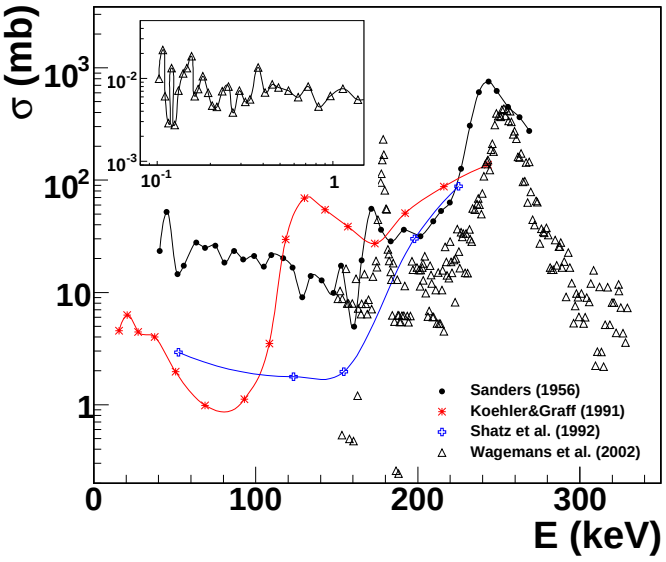

FIG. 1. The ^{17}O(n,α)^{14}C excitation function by using the experimental data available in the literature. The lines connecting the experimental data have only the aim of guiding the eye.

II. BASIC FEATURES OF THE THM

The THM is an indirect technique developed to study an astrophysically relevant reaction $a + x \rightarrow c + d$ without the need of extrapolation, usually performed in direct measurements to access the corresponding Gamow peak [16]. In particular, THM allows one to overcome the Coulomb barrier and to measure the bare nucleus cross section avoiding the electron screening as well [18–20]. For such reasons, THM has been largely applied to shed light on different issues, ranging from pure nuclear physics (as p+p proton scattering [21]) to nuclear astrophysics (as in the case of the recent ^{13}C(α,n)^{16}O, ^{17,18}O(p,α)^{14,15}N, ^{19}F(p,α)^{16}O, ^{6,7}Li(p,α)^{3,4}He, ^{10,11}B(p,α)^{7,8}Be indirect measurements [22, 23]). Although neutron induced reactions are not hindered by Coulomb barrier penetration or enhanced by electron screening, if partial waves other than s-wave are present in the entrance channel, they might be suppressed by the occurrence of the centrifugal barrier. Recently, the method has been extended to the indirect study of neutron induced reactions [17], demonstrating the possibility to bypass even the centrifugal barrier suppression effects and to pick out the contribution of the mere nuclear interaction.

The THM has its scientific background in the theory of direct reactions, and in particular in the studies of the Quasi-Free (QF) reaction mechanism [24]. Basically, these are direct processes in which the interaction between an impinging nucleus and the target can cause the *break-up* of the target (TBU) or the projectile (PBU). In particular, QF processes have three particles in the exit channel, one of which can be thought as a "spectator". Sketching for simplicity a TBU process, the picture is that of an interaction between the impinging nucleus and fraction of the nucleons forming the target (collectively called "participants"), while the other counterpart does not participate in the reaction. In this picture, the spectator will be then "free" from any effect due to the interaction between the incoming nucleus and the participant [25]. By referring to Fig.2, THM selects the QF contribution of an appropriate reaction $a + A \rightarrow c + d + s$ [26–28], performed at energies well above the Coulomb barrier, to measure the $a(x,c)d$ reaction cross section devoid of both Coulomb or centrifugal barrier suppression

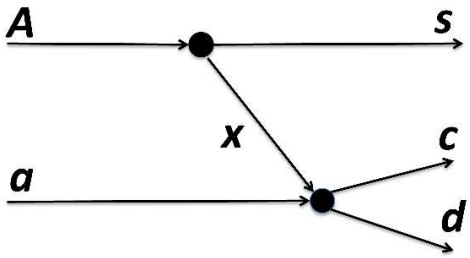

FIG. 2. Pole diagram describing the quasi-free (QF) $a+A \rightarrow c+d+s$ reaction discussed in the text. Nucleus A breaks up into fragments x and s. The former is the *participant* of the binary reaction $a(x,c)d$, while the *spectator* s does not take part to the reaction.

effects. Since the $a+A$ interaction is induced at energies well above its Coulomb barrier, no electron screening effect alters the trend of the $a+x \rightarrow c+d$ TH cross section. The QF reaction $a+A \rightarrow c+d+s$ between the projectile a and the target A, whose wave function is assumed to have a large amplitude for the $A = x \oplus s$ cluster configuration, can be described by the diagram in Fig.2 [26–28]. It represents the dominant process (pole approximation), while other processes, such as re-scattering between the reaction products, are neglected [26]. Here we briefly illustrate the theory for resonant reactions. A full account to the THM theoretical foundations can be found in [29] and references therein. In the case of resonant reactions, the lower pole of Fig.2 describes the population of the i^{th} resonant state in the F compound nucleus via the $a+x \rightarrow F_i \rightarrow c+d$ process. Thus, the $a+A$ process is described as the stripping $a+A \rightarrow s+F$ to a resonant state in the compound system F_i, which later decays to the $c+d$ channel [30, 31].
By using the PWIA approach, the TH double differential cross section can be written as [30, 32, 33]:

$$\frac{d^2\sigma^{TH}}{d\Omega_{\mathbf{k}_{sF}} dE_{cd}} = \frac{1}{2\pi} \frac{\Gamma_{cd}(E_{cd})}{(E_{cd}-E_{R_{cd}})^2 + \frac{1}{4}\Gamma^2(E_{cd})} \times \frac{d\sigma_{(a+A\rightarrow s+F)}}{d\Omega_{\mathbf{k}_{sF}}}, \quad (1)$$

where $\frac{d\sigma_{(a+A\rightarrow s+F)}}{d\Omega_{\mathbf{k}_{sF}}}$ is the differential cross section for the stripping $A(a,s)F$ reaction populating the F_i resonant state with resonance energy $E_{R_{cd}}$, $\Gamma_{cd}(E_{cd})$ is the partial resonance width for the $F \rightarrow c+d$ decay, Γ is the total resonance width and $E_{ij} = k_{ij}^2/(2\mu_{ij})$ is the relative kinetic energy of the particle i and j, with μ_{ij} their reduced mass.

III. THE EXPERIMENT

A. Experimental Setup

The ^{17}O$(n,\alpha)^{14}$C reaction has been studied via the ^{2}H$(^{17}O,\alpha^{14}C)^1$H three body process, where deuteron has been chosen as TH-nucleus owing to its obvious $p-n$ structure and its well-known radial wave function for the intercluster motion, given by the Hulthén function [16, 34]. In QF framework, the emerging proton represents the *spectator* while the neutron is the *participant* to the binary reaction in the lower pole, populating the ^{18}O* excited levels.
Two experiments were performed, both using ^{2}H to populate ^{18}O excited states. The first experiment was performed at Laboratori Nazionali del Sud (LNS), located in Catania, Italy. A second experiment was performed at the Nuclear Science Laboratory (NSL) of the University of Notre Dame, South Bend (Indiana, USA). For sake of brevity, we will describe in more detail the most recent experiment, because the same experimental and data analysis procedures were used in the two.
The JN Tandem Van der Graaf provided a 43.5 MeV ^{17}O beam impinging on a thin self-supported deuterated polyethylene (CD_2) target, about 170 μg/cm^2 thick, placed at 90° with respect to the beam direction. A schematical view of the used detection setup, symmetric with respect to the beam axis, is shown in Fig.3. It consisted of two telescopes (DE1-A1 and DE2-B1), optimized for ^{14}C detection, each one made of an ionization chamber (IC) and a 1000μm thick silicon Position Sensitive Detector (PSD). The telescopes were placed at a distance of about 480 mm from the target covering the angular ranges 7.5°±2.5°. The ionization chambers were used to discriminate carbon nuclei by means of the standard $\Delta E - E$ technique. The ICs, with isobutane flowing with an approximately pressure of 50 mbar, had an energy resolution of ≈10%. Such pressure was enough to discriminate particles by their charge but not their mass. Two thin mylar foils respectively of 0.9μm and 1.5μm were used as entrance and exit windows of each IC. Their thickness was chosen to minimize the angular straggling. Four additional 500μm PSDs referred to as A2, A3, B2 and B3 were optimized for alpha particles detection. A2 and B2 were placed at a distance of about 480 mm from the target, covering the angular ranges 17.5°±2.5° while A3 and B3 were placed at about 390 mm from the target covering the angular range 27.3°±3.5°. The distances were chosen to keep the intrinsic angular resolution better than 0.1°, allowing at the same time to cover the relevant angular regions for the subsequent analysis. Angular conditions were selected to cover the phase-space region where momentum values of the undetected proton range from 0 up to ∼150 MeV/c. In this way, the region around p_s=0 MeV/c is fully covered, where the p-n momentum distribution is maximum, since p-n motion inside deuteron predominantly takes place in s-wave.
Energy and position signals for the detected particles

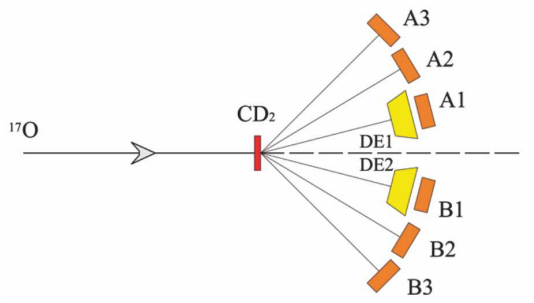

FIG. 3. Sketch of the experimental setup. The ^{17}O beam was impinging on a CD_2 target. The emitted particles were detected by four PSDs (A2, A3, B2 and B3) and by two ΔE-E telescopes (DE1-A1 and DE2-B1).

were processed by standard electronics and sent to the acquisition system, allowing for on-line monitoring of the experiment and the data storage for off-line analysis. Coincidences (logic AND) among either one of the two forward telescopes and one of the three placed PSD detectors (logic OR) on the opposite side with respect to the beam axis were used as trigger for the ACQ system.

B. Calibration

At the initial stage of the measurement, an equally spaced grid was mounted in front of each PSD to perform angular calibration. The angle of each slit with respect to the beam direction was determined by using an optical system, making it possible to establish a correspondence between position signal from the PSDs and detection angle of the impinging particles. Position and energy calibration runs were performed by using ^{4}He and ^{12}C beams scattered off a 93μg/cm^2 thick ^{197}Au target at energies from 5 up to 50 MeV, to measure the elastic scattering peaks at several energies. This allowed an accurate calibration of PSDs A1 and B1, optimized for carbon nuclei detection, and of the ICs, by difference in the residual energy measured by PSDs when the ICs were empty and filled with isobutane at the working pressure. The total kinetic energy of the detected particles was reconstructed off-line, taking into account the energy loss in the target and in the entrance and exit windows of the ionization chamber and in the other dead layers. Angular and energy resolution have been evaluated to be less than 0.1° and 1%, respectively.

C. Reaction Channel Selection

After detector calibration, the three-body ^{2}H(^{17}O,$\alpha^{14}C$)^{1}H reaction channel of interest was separated from others, induced by the interaction of ^{17}O with other elements in the target (C, H, O, for instance). This was accomplished by studying the events

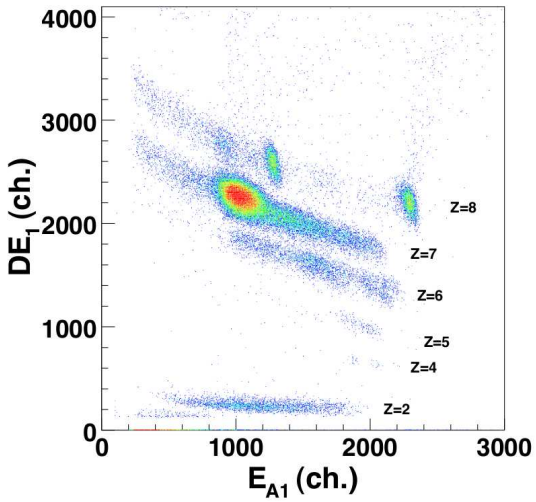

FIG. 4. $\Delta E - E$ matrix for C identification in the DE1-A1 telescope. The DE2-B1 telescope provides similar result.

corresponding to a carbon particle detected in one of the two $\Delta E - E$ telescopes in coincidence with any particles on an opposite silicon detector. The emerging proton was not detected in the present experiment, since its kinematics can be easily deduced by means of energy and momentum conservation laws [15, 29]. The selection of the carbon isotopes (Z=6) by means of the standard $\Delta E - E$ technique is reported in Fig.4.
As already mentioned, only two of the three emitted particles were detected. This might leave the system underdetermined due to the overlapping of different kinematic loci in the same phase-space region, corresponding to reactions having different undetected particles. To identify the mass of the undetected particle s, the procedure discussed by [35] was applied. Since its momentum is deduced from the energies and emission angles of alpha particles and ^{14}C nuclei by applying the momentum conservation equation, the variable $X = p_s^2/2u$ is independent of the mass of the undetected fragment s (u being the unit mass in a.m.u.). If we define $Y = E_{beam} - E_\alpha - E_{^{14}C}$, the energy conservation equation can be cast in the form:

$$Y = \frac{1}{A_s} X - Q_{2\to 3}, \qquad (2)$$

thus the mass of particle s can be inferred by fitting the line that best reproduces the experimental data. Its application is demonstrated in figure 5 for the actual ^{2}H(^{17}O,α^{14}C)^{1}H reaction and the A1-B2 coincidence detectors, similar results are obtained for the other detector couples. Clearly, events gather along a straight line whose slope is 1, allowing us to assert that no additional channels contribute to the experimental kinematic locus. By means of the energy conservation law and by considering an *undetected particle* having mass 1 a.m.u., the experimental Q-value spectrum for the selected events was also reconstructed and the corresponding result shown in

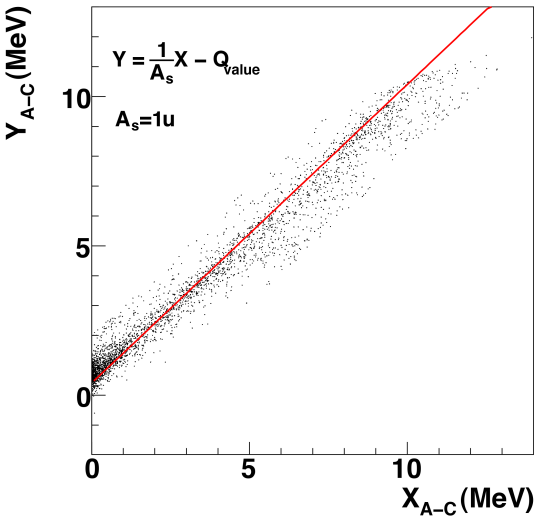

FIG. 5. Identification of particle s according to the procedure described in [35], applied to the A1-B2 coincidences. In axes, $Y = E_{beam} - E_c - E_C$ and $X = p_s^2/2u$, where E_c and E_C are the energies of α and ^{14}C nuclei, while p_s is the momentum of the undetected particle s from momentum conservation. Energy conservation implies $Y = \frac{1}{A_s}X - Q_{2\to3}$; thus, the mass of s can be determined.

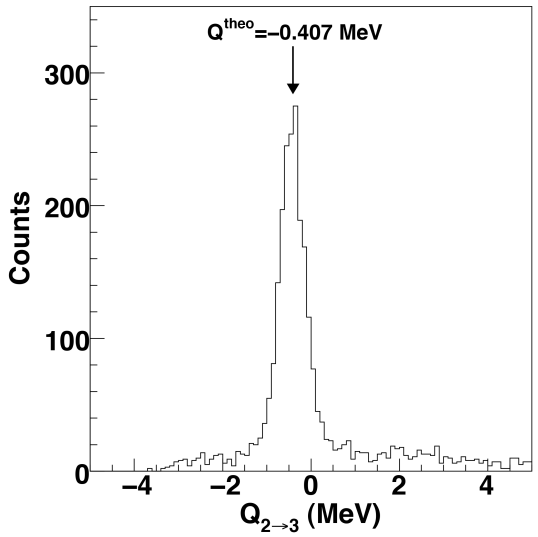

FIG. 6. Experimental Q-value spectrum. A single peak shows up, whose centroid agrees well with the theoretical Q-value of -0.407 MeV for the ^{2}H(^{17}O,α^{14}C)^{1}H reaction.

Fig.6. The prominent peak, centered at about -0.4 MeV, clearly demonstrates that no other reaction channels influence the one of interest here, being background lower than 7% with respect to the total statistics. The good agreement between the centroid of the experimental Q-value spectrum of Fig.6 and the expected value of -0.407 MeV, marked by the black vertical arrow, is also a signature of our good calibration.

Since the kinetic energies of the outgoing particles are correlated by energy and momentum conservation laws, the experimental kinematical locus $E_{^{14}C}$.vs.E_α was extracted and compared with detailed kinematical calculations in which detection angles, detection thresholds, and energy losses have been included. The result is shown in Fig.7, displaying the experimental kinematical locus (red points) for three different angular conditions spanned by the detectors A_1 and B_2 of Fig.3 as compared with the kinematical calculations (black points). The good agreement between the experimental data and the simulated spectra for different detection angular pairs strongly confirm the good selection of the ^{2}H(^{17}O,α^{14}C)p reaction channel.

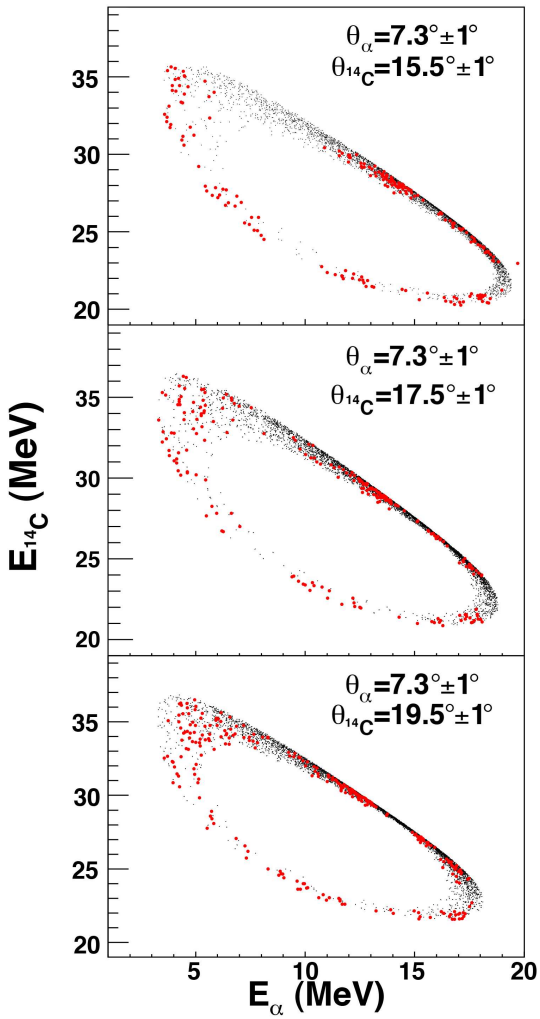

FIG. 7. The $E_{A1} - E_{B2}$ kinematical loci for three different angular conditions marked in the pictures. The experimental data (red points) are compared here with simulated ones for the ^{2}H(^{17}O,α^{14}C)^{1}H reaction channel (black points).

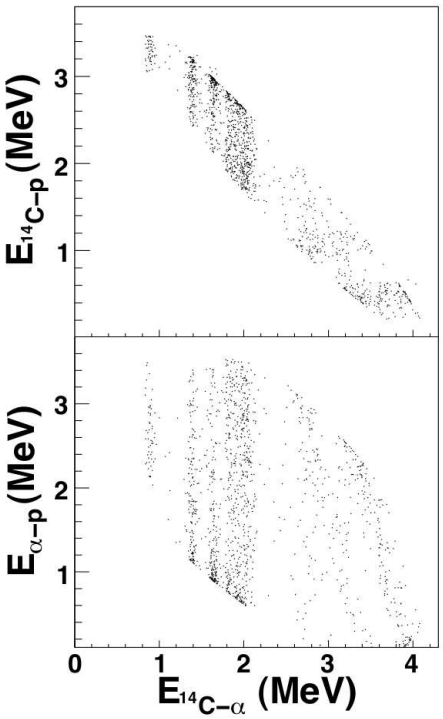

FIG. 8. Two dimensional plot for the ^{14}C-p and α-p relative energies as a function of the ^{14}C-α one. Very clear vertical loci are detectable, due to the population of the 7.114 MeV (J^π=4^+), 7.620 MeV (J^π=1^-), 7.864 MeV (J^π=5^-), 8.039 MeV (J^π=1^-), 8.121 MeV (J^π=5^-), 8.224 MeV (J^π=2^+), and 8.289 MeV (J^π=3^-) ^{18}O excited levels.

D. Selection of the QF Reaction Mechanism

A further study on reaction dynamics is necessary to select those kinematical regions where QF mechanism is dominant and can be separated from others, feeding the same particles in the final state. This is an essential step because the equations we have briefly discussed are valid only under the assumption that particle s, namely the proton, acts as a spectator to the $A-x$ interaction. To this aim, relative-energy correlation plots for α-p, ^{14}C-p and ^{14}C-α systems were deduced from the measured energies and emission angles. Of course, the relative energy spectra represent the excitation energy spectra for ^{5}Li, ^{15}N and ^{18}O nuclei, respectively save a constant term (the breakup threshold). It means that if any state in such compound systems has been fed in the investigated phase-space region, a bump in the reaction yield should show up at the energy corresponding to the populated excited level.

The $E_{^{14}C-p}$ and $E_{\alpha-p}$ relative energies are displayed in Fig.8 as a function of the $E_{^{14}C-\alpha}$ relative energy, in the upper and lower panels, respectively. In both panels of Fig.8, different vertical loci are clearly visible, being these events corresponding to the ones coming from the population of the 7.114 MeV (J^π=4^+), 7.620 MeV (J^π=1^-), 7.864 MeV (J^π=5^-), 8.039 MeV (J^π=1^-), 8.121 MeV (J^π=5^-), 8.224 MeV (J^π=2^+), and 8.289 MeV (J^π=3^-) ^{18}O excited levels. The correspondence between the horizontal axis of Fig.8 and the ^{18}O excitation energy can be easily found if the α-^{14}C$\rightarrow^{18}$O threshold energy of 6.227 MeV, given in [36], is taken into account.

In the upper part of Fig.8, two horizontal loci are also observed, due to events coming from ^{15}N excited levels population. However, even if they constitute a sequential decay to be further investigated, they do not contribute to the reaction yield in the energy region of interest for the present work, namely 1.2 MeV$\leq$E$_{^{14}C-\alpha}\leq$2.2 MeV. On the contrary, no evidence of the population ^{5}Li levels was detected.

As a further study to discriminate the reaction mechanism intervening in the present experimental data, the coincidence yield has been studied as a function of the proton momentum p_s. Indeed, an enhancement of the cross section close to zero proton momentum is a necessary condition for the occurrence of the QF mechanism, marking the presence of a modulation of the TH cross section by the proton momentum distribution inside the deuteron. This feature is expected for a QF reaction because the momentum distribution of the $n-p$ system inside the deuteron has a maximum for p_s= 0 MeV/c. Since the experimental range of the spectator particle momentum extends well beyond the interval where the QF contribution is supposed to be dominant, a comparison of the coincidence yield for small p_s and larger p_s can be performed. For this purpose, the behavior of the coincidence yield spectra as a function of $E_{c.m.}$ was reconstructed for all coincidence events, for different proton momentum ranges. $E_{c.m.}$ is given by:

$$E_{c.m.} = E_{^{14}C-\alpha} - Q_2, \tag{3}$$

where $E_{^{14}C-\alpha}$ is the relative energy between the detected α and C particles and Q_2=1.817 MeV is the Q-value of the ^{17}O(n,α)^{14}C reaction. In detail, these spectra, given in figure 9, were obtained by selecting the $|p_s|$ <20 MeV/c (upper panel), 20 Mev/c < $|p_s|$ < 40 MeV/c (middle panel) and 40 MeV/c < $|p_s|$ < 60 MeV/c (lower panel) intervals of the proton momentum p_s. Furthermore, such spectra were divided by the phase-space contribution to remove phase-space effects. In the picture, only the $E_{c.m.}$ range of interest is displayed, namely $E_{c.m.}$ <0.4 MeV; here, the four ^{18}O resonances reported in table I show up. The picture clearly demonstrates that the coincidence yield is much higher for $|p_s|$ <20 MeV/c than what is obtained at larger p_s momenta. Indeed, at higher momenta (20< $|p_s|$ <40 MeV/c and 40< $|p_s|$ <60 MeV/c) it drastically decreases and the resonances become barely visible compared to background. These data provide strong evidence of a clear correlation between coincidence yield and spectator momentum p_s, which is a necessary condition for the occurrence of the QF reaction mechanism.

An observable more sensitive to the reaction mechanism is the shape of the momentum distribution for the $p-n$ intercluster motion in the deuteron. Indeed,

TABLE I. Summary of the ^{18}O resonances in the energy range explored in the experiment. The $^{18}O^*$ values are taken from [7]

	$^{18}O^*$ (MeV)	$E_{c.m.}$ (keV)	J^π
1	8.039	-6	1^-
2	8.121	75	5^-
3	8.224	178	2^+
4	8.289	244	3^-

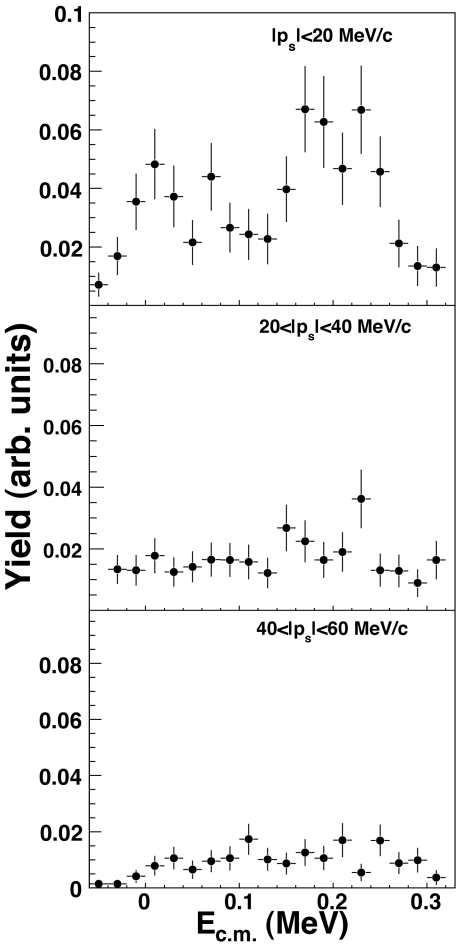

FIG. 9. Normalized reaction yield for different p_s ranges. The reaction yield monotonically decreases moving to high p_s values, as expected for a QF reaction using deuteron as TH nucleus. This represent a first test of the occurrence of the QF mechanism in the $^{17}O(n,\alpha)^{14}C$ reaction.

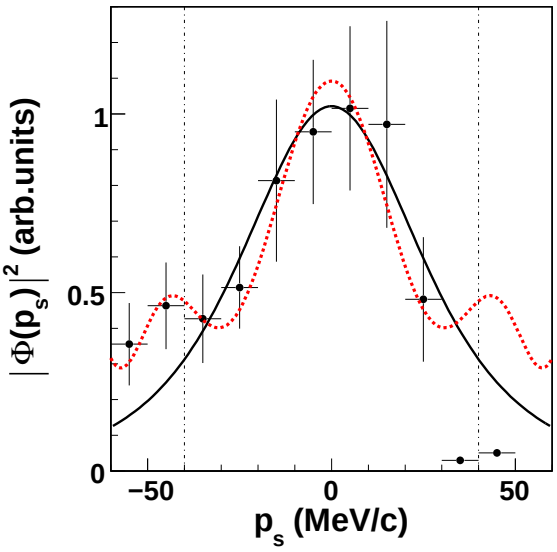

FIG. 10. Experimental momentum distribution (black points), compared with the theoretical Hulthén function in momentum space (red line).

only if the deuteron breakup is direct, the proton momentum distribution keeps the same shape as inside d. The experimental momentum distribution was extracted by selecting the events corresponding to the most populated resonance in the TH measurement at energy 8.224 MeV, $E_{c.m.}$=178 keV. The resulting quasi-free yield is divided by the kinematical factor that takes in account the covered angular ranges of the experiment and the detection thresholds. The experimental momentum distribution was then compared with the square of a Hulthén wave function in momentum space [37] that represents the shape of the $n-p$ momentum distribution in the Plane-Wave Impulse Approximation (PWIA), given by:

$$\Phi(p_s) = \frac{1}{\pi}\sqrt{\frac{ab(a+b)}{(a-b)^2}}\left[\frac{1}{a^2+p_s^2} - \frac{1}{b^2+p_s^2}\right], \quad (4)$$

with parameters a=0.2317 fm^{-1} and b=1.202 fm^{-1} for deuteron [37]. The experimental momentum distribution is shown in Fig.10 by black dots while the solid line represents the squared Hulthén wave function in momentum space. The experimental momentum distribution extracted here returns a FWHM of 58±11 MeV/c, in good agreement with the theoretical value of $\sim$ 60 MeV/c.

The correspondence, within $|p_s|$ <40 MeV/c, between the experimental data and the theoretical function, together with the previous tests, makes us confident that the QF mechanism gives the main contribution to the reaction in the considered p_s range. To check if the simple PWIA approach gives an accurate description of the $p-n$ momentum distribution, the experimental data are also compared with the distribution determined in the Distorted Wave Born Approximation (DWBA) framework [38] (red dashed line in Fig.10) using the FRESCO

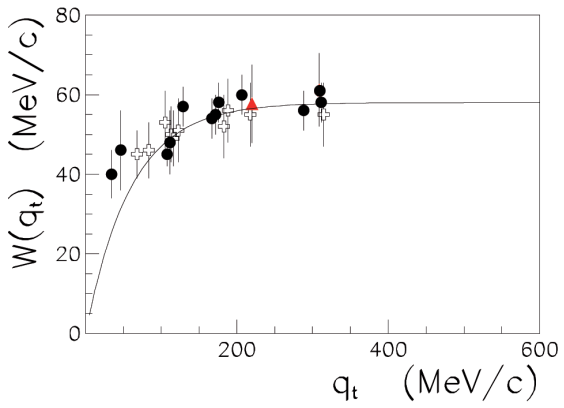

FIG. 11. Trend of the FWHM of the p-n momentum distribution measured in THM experiments as function of the correspongin trasferred momentum defined as in Pizzone *et al.* 2009 [42], i.e. larger transferred momentum values agree with the asymptotic value of the FWHM. The red triangle show the FWHM measured in the present work.

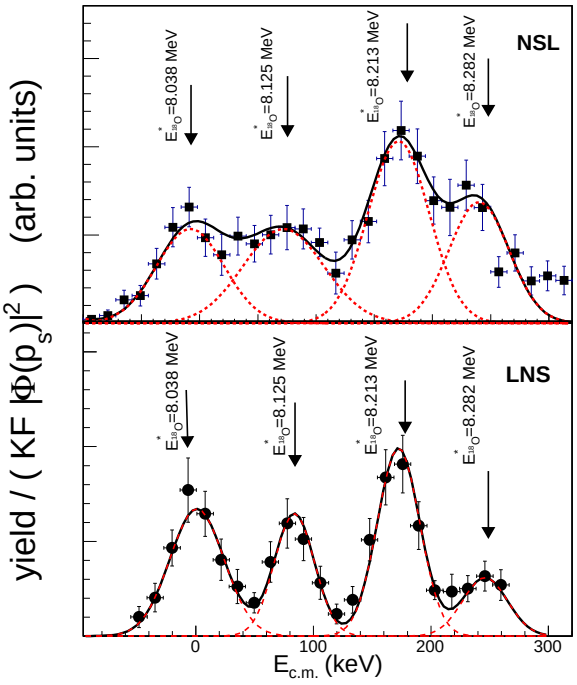

FIG. 12. Experimental THM data, referring to the center-of-mass angular range covered in the present experiment, i.e. $40°<\theta_{c.m.}<90°$ (NSL data) and $50°<\theta_{c.m.}<60°$ (LNS data).

code [39]. In the calculation, optical potential parameters adjusted from the Perey and Perey compilation [40] were adopted, varying the optical potential parameters in the entrance and exit channels by 30% at most, since there are no available optical potentials at the low energies involved in the studied reaction. From the comparison in Fig.10, we can state that a good agreement between DWBA and PWIA is present, within the experimental uncertainties, for neutron momentum values lower than ∼40 MeV/c. The vertical dot-dashed lines in Fig.10 mark the position of the selected events for which the TH will be applied [16, 22, 30, 31]. Using a gaussian fit of the experimental momentum distribution, we deduced the FWHM. Since in the present experiment the transferred momentum was ∼55 MeV/c, this data point was inserted in the FWHM vs. transferred momentum plot as explained in [41, 42], thus confirming once again the PWIA hypothesis. Similar results have been found in the LNS experiment [17].

IV. THE THM TRIPLE DIFFERENTIAL CROSS SECTION

So far we have focused on the data taken at NSL. As already mentioned, a similar analysis was performed on the data taken at LNS. In this experiment, a setup similar to the one arranged for the NSL experiment was used, with a beam energy of 41 MeV (as already extensively reported in [17]). After validating the results, we will aggregate the whole set of data, given they are compatible, as we will show in the following section, to improve the statistics and reduce possible systematic errors.

The same tests and analysis procedure was applied to the data from this experiment, and similar results were obtained. In this case a momentum cut $|p_s|$ <40 MeV/c was adopted as well.

The selected events are shown as black squares in Fig.12 for the NSL experiment, with their statistical error of about 13% (upper panel). The LNS data are shown as black points in the low panel of Fig.12, instead. In both cases, the superimposed black-lines represent a fit of the data, performed with the sole aim of establishing the relative weight of each resonance in the total reaction yield as a function of the variable $E_{c.m.}$. The separation of the contribution is important to perform the angular distribution integration.

It is worth noticing that the experimental resolution dominates over the natural width of the measured ^{18}O resonant levels, returning a common value of about 50 keV (FWHM) for the NSL experiment and of about 35 keV (FWHM) in the case of the LNS experiment in the coincidence yield of Fig.12. Those values correspond to the predicted uncertainty on the $E_{c.m.}$ variable if the beam energy straggling in the target, the intrinsic angular and energy resolution of the silicon detectors, the angular and energy straggling of the detected α and ^{14}N particles (in both target and dead layers) are taken into account when calculating the final error on Eq.3 by means of the standard error propagation procedure.

The coincidence yield is dominated by the 8039 keV (J^π=1^-), the 8121 keV (J^π=5^-), the 8224 keV (J^π=2^+), and the 8289 keV (J^π=3^-) ^{18}O excited levels [7],

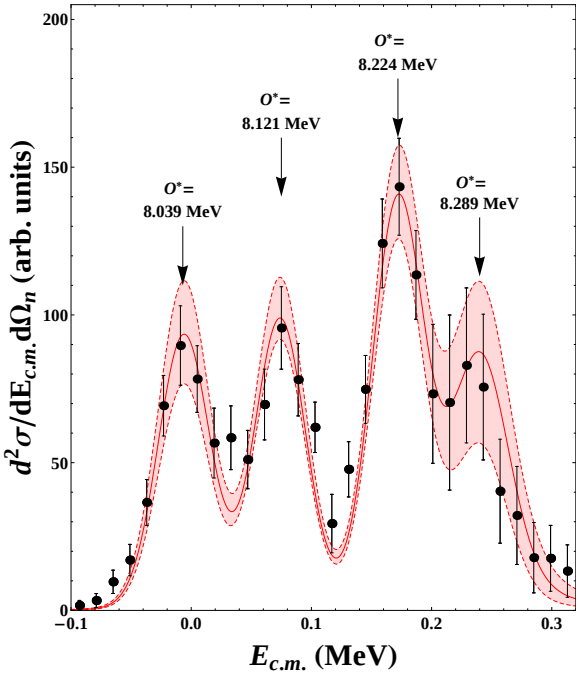

FIG. 13. QF cross section of the ^{2}H(^{17}O,α^{14}C)^{1}H reaction in arbitrary units. The black points are the experimental data with the vertical error bars taking into account the statistical and angular distribution integration uncertainties. The line represents the best fit to the data calculated in the modified R-matrix approach, normalized to the peaks at about 178 and 244 keV.

producing a subthreshold resonance at -6 keV and resonances at 75 keV, 178 keV, and 244 keV in the two-body ^{17}O(n,α)^{14}C cross section, respectively. While for the resonances at -6 keV, 178 keV and 244 keV spectroscopic information are available in the literature [8, 10, 11], for the 75 keV resonance in the ^{17}O-n system no information are available at present. Indeed, its population is strongly hampered in the ^{17}O-n entrance channel owing to the centrifugal barrier, since n-destruction takes place in d-wave.

V. OBTAINING SPECTROSCOPIC INFORMATION FROM THE THM CROSS SECTION

The experimental yield shown in Fig.12 refers only to a small $\theta_{\rm c.m.}$ angular range, being it defined in the center-of-mass of the subreaction ^{17}O+n$\rightarrow \alpha+^{14}$C, as the angle between the momentum of any of the two fragments (α or ^{14}C) and the virtual beam direction,

$$\theta_{\rm c.m.} = \arccos(\hat{\mathbf{k}}_{\rm n^{17}O}\cdot\hat{\mathbf{k}}_{\alpha^{14}\rm C}). \quad (5)$$

In the previous formula, $\hat{\mathbf{k}}_{\rm ij}=\frac{\mathbf{k_{ij}}}{k_{ij}}$ are the relative momenta between particles i and j. Since the THM data sets correspond to different center-of-mass $\theta_{\rm c.m.}$ ranges of 40°-90° (NSL experiment) and 50°-60° (LNS experiment), integration over the whole angular range has to be performed before comparing the data sets and combining them in a single one by means of the already published angular distribution of Gulino *et al.* 2013 [17] for the 8039 keV (l=1), the 8121 keV (l=3), the 8224 keV (l=2), and the 8289 keV (l=1) respectively, through the standard formula

$$\Xi_i = \frac{\int_{\theta^{\rm min}_{\rm c.m.}}^{\theta^{\rm max}_{\rm c.m.}} \frac{d\sigma}{d\Omega}(\theta_{\rm c.m.})d\Omega}{\int_{\theta^{0}_{\rm c.m.}}^{\theta^{\pi}_{\rm c.m.}} \frac{d\sigma}{d\Omega}(\theta_{\rm c.m.})d\Omega} \quad (6)$$

where the integration of the experimental angular distributions $\rm d\sigma/d\Omega(\theta_{c.m.})$ has been performed in the angular range ($\theta^{\rm min}_{\rm c.m.}$,$\theta^{\rm max}_{\rm c.m.}$). Then, each resonance contribution to the THM cross section, disentangled by means of the fits given in Fig.12, has been divided by these factors to determine the angular integrated cross section $\rm d^2\sigma/dE_{c.m.}d\Omega_n$. The resonance deconvolution procedure introduces an uncertainty of about ∼11% to the overall error budget because of the energy resolution effects on the experimental data of Fig.12. Finally, the good agreement between the two THM measurements, within the experimental uncertainties (as shown in Fig.12), allowed us to avarage the two data sets, weighing over the respective errors, in order to improve statistics and data quality. The two data sets differ significantly only in the energy range characterized by the presence of the 8282 keV level. This discrepancy is due to the different kinematical range covered in the two experimental setups [17]. To overcome this problem in that energetic region the final data are characterized by a bigger error bar (of about 20%) containing the upper and lower limit of the errors of each data sets.

The procedure described above leads to the result of Fig.13 where the black-points (with their only statistical error bars) represents the THM cross section integrated over the whole $\theta_{c.m.}$ range.

Once the THM cross section has been extracted, it has been possible to determine the reduced widths of the involved resonant levels by means of the formula already given in Eq.1. In particular, following the PWIA prescription for isolated non-interfering resonances, Eq.1 can be written in a similar form in which the reduced widths γ explicitly appear, taking the form [31, 33]

$$\frac{\rm d^2\sigma}{\rm dE_{xa}d\Omega_s} = \rm NF \times \sum_i (2J_i+1) \times \left| \sqrt{\frac{k_f(E_{xa})}{\mu_{cd}}} \frac{\sqrt{2P_{l_i}(k_{cd}R_{cd})}M_i(p_{xa}R_{xa})\gamma^i_{cd}\gamma^i_{xa}}{D_i(E_{xa})} \right|^2 \quad (7)$$

where NF is a normalization factor, $k_f(E_{xa}) = \sqrt{2\mu_{cd}(E_{xa}+Q_2)}/\hbar$, P_{l_i} the penetration factor in l_i-wave, R_{xa} and R_{cd} the channel radii. Here, the channel radii have been fixed by using the standard formula $\rm R=1.3(A_1^{1/3}+A_2^{1/3})$ fm, thus leading to $\rm R_{n^{17}O}$=4.64 fm

TABLE II. Summary of the ^{18}O resonant states observed in this experiment. For comparison, resonance parameters from Wagemans *et al.* 2002 [8] are shown as well (marked by the "dir." superscript). For the negative-energy resonance in direct data, the reduced with (rw) is given.

$E_{c.m.}$ (keV)	Γ_n^{THM} (eV)	Γ_α^{THM} (eV)	Γ_{tot}^{THM} (eV)	$\Gamma_n^{dir.}$ (eV)	$\Gamma_\alpha^{dir.}$ (eV)	Γ_{tot}^{dir} (eV)
-6	0.01±0.001	2400±300	2400±300	27 (rw)	2399	2400
75	0.05±0.006	36±5	36±5	—	—	—
178	86±11	2200±300	2260±300	76±4	2182±132	2258±135
244	1700±450	13000±3400	14700±3800	1078±22	13661±416	14739±590

and $R_{\alpha^{14}C}$=5.20 fm. The uncertainties due to the ambiguity on the channel radii was here evaluated by changing $R_{n^{17}O}$ and $R_{\alpha^{14}C}$ by 10%, giving a difference in the calculations of about 5%, so it has been neglected in the following analysis.

$$M_i(p_{xa}R_{xa}) = \left[(B_{xa\,i}-1)\,j_{l_i}(\rho) - \rho\frac{\partial j_{l_i}(\rho)}{\partial\rho}\right]_{\rho=p_{xa}\,R_{xa}} \quad (8)$$

[43], where $j_{l_i}(\rho)$ is the spherical Bessel function, $p_{xa} = \sqrt{2\mu_{xa}(E_{xa}+\epsilon_{xs})}/\hbar$ (ϵ_{xs} the binding energy of the $A = (x\,s)$ system), and $B_{xa\,i}$ an arbitrary boundary condition chosen as in [44] to yield the observable resonance parameters. Finally, $D_i(E_{xA})$ is the standard R-matrix denominator in the case of one-level, two-channel R-matrix formulas [45].

By using such input parameters in Eq.7 and taking also into account the experimental FWHM resolution of 40 keV on the $E_{c.m.}$ variable, the normalization factor NF appears as the only free parameters to adjust the Half-Off-Energy-Shell (HOES) R-matrix calculation to the experimental THM data of Fig.13, expressed in arbitrary units. This factor was obtained by scaling the THM cross section to the data in the energy range above 130 keV in the center-of-mass system where the well known resonances at 8224 keV and 8282 keV are dominant, by following the procedure applied in La Cognata *et al.* [44]. Moreover, the use of a broad energy interval minimize the systematic effects [46].

Once NF was fixed, this scaled modified R-matrix calculation has been used to fit the THM resonances, thus allowing to determine the corresponding neutron γ_n and alpha γ_α reduced widths, left as the only free parameters in the calculation. The solid red line displayed in Fig.13 represents the modified R-matrix fit to the experimental data, for which a reduced chi-square of $\tilde{\chi}$=0.8 has been found. The red band in Fig.13 accounts for the error introduced by the normalization procedure, evaluated here at about 15%.

Eq.8 demonstrates that the same reduced widths γ appear in direct and THM cross sections, therefore the reduced widths extracted from R-matrix fit on the THM can be inserted in Eq.8 to reproduce the available direct data cross section. It must be stressed here that the reduced γ-widths for the two highest levels have been determined to reproduce the partial widths given in Wagemans *et al.* [8] and Avila *et al.* [7]. In particular, for the 8224 keV the values of Γ_n=86±11 eV and Γ_α=2171±282 eV have been considered (as given in [8] and [7]), while for the 8289 keV the values of Γ_n=1714±446 eV and Γ_α=13021±3386 eV have been extracted, being these in reasonable agreement within two sigma with the one give in [8] but disagree with the ones determined in [7], where the authors changed the parameters in order to reproduce simultaneously the ^{14}C(α,n) channel and the ^{14}C(α,α) one [7].

By using these normalization points, it has been possible for the first time to get information about the neutron and alpha partial widths of the 75 keV resonant level, corresponding to the ^{18}O 8125 keV excited state. To get such values, and since J^π conservation rules require d-wave neutrons, the fit has been performed by maintaining $\Gamma_n << \Gamma_\alpha$, thus leading to the values of Γ_n^{THM}=0.050±0.006 eV and Γ_α^{THM}=36±5 eV. The values obtained here lie within 15% of the Wigner limit and, with particular regard to the reduced γ_α-width, it is well inside the upper limit given in the work of Gai *et al.* [47], Γ_α <260 eV.

It is worth of notice here that due to the features of the THM, it has been possible to calculate also the Γ_n^{THM} of the subthreshold level (8039 keV) while only the reduced width (rw) is given in the literature [8]. This level contributes significantly to the total cross section and it is fundamental for the astrophysical intent.

VI. REACTION RATE AND CONCLUSIONS

From the modified R-matrix calculation shown in the previous section, it is possible to calculate the total reaction rate by means of the standard formula [48]:

$$N_A\langle\sigma v\rangle = \frac{3.7318\times10^{10}}{T_9^{3/2}}\sqrt{\frac{A_1+A_2}{A_1A_2}}\times \\ \times\int_0^\infty E\sigma(E)e^{-11.605E/T_9}dE \quad (9)$$

where the energy E is expressed in units of MeV, A_i is the atomic mass in a.m.u., σ is the cross section in barn and T_9 is the temperature in GK ($T_9 \equiv T/10^9K$). Then, the reaction rate $N_A\langle\sigma v\rangle$ in units of $cm^3mol^{-1}s^{-1}$, being N_A the Avogadro number and $\langle\sigma v\rangle$ is the convolution of the cross section with the Maxwell distribution in Eq.9.

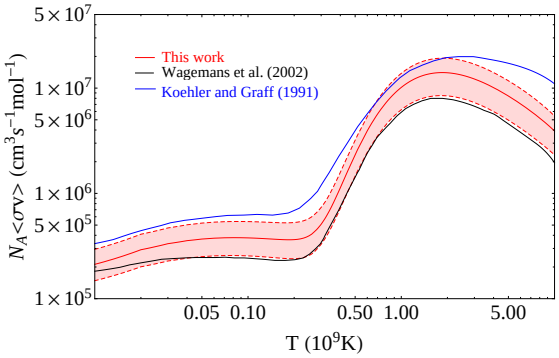

FIG. 14. The THM reaction rate (red band), compared with the others by Koehler and Graff [10] (blue line) and by Wagemans *et al.* [8] (black line).

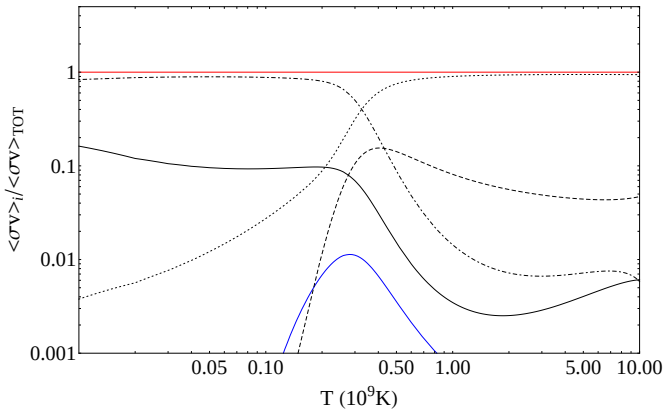

FIG. 15. Contribution of each resonant state to the total reaction rate. At low temperature, the rate is strongly affected by the subthreshold level (dot-dashed line) rather than the $1/v$ shape (black line). The major part of the contribution at high energy comes from the 244 keV level (dotted line) while the 178 keV level (dashed line) has a maximum contribution of 20%. As expected the 75 keV level (blue line) gives a contribution less than 1% due to its angular momentum.

The calculation result is shown in Fig.14 with a red line, while the red band highlights the region allowed by uncertainties (statistical and normalization) of about 20%. In Fig.14 the reaction rates obtained by Koehler and Graff [10] (blue line) and by Wagemans *et al.* [8] (black line) are also displayed. The result clearly shows that at astrophysically relevant temperatures our calculation lies in between the two previous results available in the literature.

To disentangle the contribution of each resonance state to the total reaction rate, their ratio to the total reaction rate is shown in Fig. 15. First of all, we underscore that the black solid line is used for the $1/v$ contribution, which is significant only at lowest temperatures (black line). The 75 keV level (blue line) contributes for about 1% on the total reaction rate while the subthreshold level (dot-dashed line) strongly affects the reaction rate at the temperatures relevant for astrophysics ($0.01< T_9 <1.5$). At higher temperatures, more than 80% of the contribution is due to the 244 keV level (dotted line), at odds with the claim by Wagemans *et al.* [8] because of the new angular momentum assignment.

In conclusion, the ^{17}O$(n,\alpha)^{14}$C reaction was studied by means of the THM applied to the ^{2}H$(^{17}$O,α^{14}C$)^1$H process. This is an extension of the THM to the neutron induced reactions. In this measurement, it was possible to observe the subthreshold level centered at -7 keV in the center-of-mass system corresponding to the 8.039 MeV level of ^{18}O, which is important to determine the ^{17}O$(n,\alpha)^{14}$C reaction rate. Moreover, the use of deuteron as a source of virtual neutrons allowed us to populate the level centered at 75 keV in the ^{17}O-n center-of-mass system, corresponding to the 8.121 MeV level of ^{18}O. Due to its J^π assignment (J^π=5$^-$), the population of such level is suppressed in direct measurements because of its l=3 angular momentum. The application of the modified R-matrix approach allowed us to determine the neutron and alpha partial widths of the resonance in the -10 keV÷250 keV $E_{c.m.}$ energy range, which are in agreement with the ones available in literature where available, or extracted for the first time in the case of the 8.121 MeV level.

Finally, after the calculation of the total cross section and its normalization to direct data it was possible to calculate the reaction rate. Due to the very good quality of the resonance parameters obtained by Wagemans *et al.* [8] for the 8224 keV and 8289 keV levels, we calculate a recommended rate merging the resonance widths of direct data in the region above 100 keV in the center of mass system and the results from our THM measurement at low energy, characterized by the presence of the subthreshold level that strongly affect the total reaction rate. We also consider in the calculation the modern values of the ^{18}O* excitation level as recently found in Avila *et al.* [7].

This result, shown in Fig.16, may change significantly the abundance ratios of the element involved in the nucleosynthesis network of the weak component of the *s*-process. Therefore, extensive calculations are undergoing to understand the consequences of the present results on astrophysics.

VII. ACKNOWLEDGMENTS

This work was partially supported by the Italian Ministry of the University under Grant No. RBFR082838 and "LNS AstroFisica Nucleare (fondi premiali)". A.M.M. acknowledges the support by the US DOE under Grant Nos. DE-FG02-93ER40773, DEFG52-09NA29467 and DE-SC0004958 and NSF under Grant No. PHY-0852653. J.M. acknowledges the support of the AMVIS Project under Grant No.M10480902 and LH11001 and of

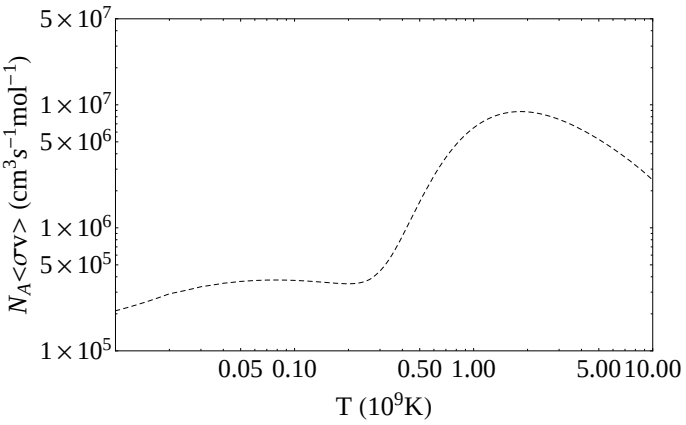

FIG. 16. Total reaction rate of the ^{17}O(n,α)^{14}C reaction calculated merging the best results of Wagemans *et al.* [8] in the energy region above 100 keV in the center of mass system and the result coming from THM measurement at low energy.

the GACR Project under Grant No. P203/10/0310. The Notre Dame collaborators were supported by the NSF under Grants No. PHY-0758100 and No. PHY-0822648. The authors acknowledge also the staff of the NSL and LNS accelerator divisions and the LNS target laboratory.

[1] M.-S. Yim and F. Caron, Progress in Nuclear Energy, **48**, 2 (2006).
[2] T. Kajino, Nuclear Physics A, **588**, 339 (1995).
[3] J. H. Applegate, C. J. Hogan, and R. J. Scherrer, Astrophys. J., **329**, 572 (1988).
[4] F. Käppeler, R. Gallino, S. Bisterzo, and W. Aoki, Reviews of Modern Physics, **83**, 157 (2011), arXiv:1012.5218 [astro-ph.SR].
[5] M. Pignatari, R. Gallino, M. Heil, M. Wiescher, F. Käppeler, F. Herwig, and S. Bisterzo, Astrophys. J., **710**, 1557 (2010).
[6] F. Ajzenberg-Selove, Nucl. Phys. A, **475**, 1 (1987).
[7] M. L. Avila, G. V. Rogachev, E. Koshchiy, L. T. Baby, J. Belarge, K. W. Kemper, A. N. Kuchera, and D. Santiago-Gonzalez, Phys. Rev. C, **90**, 042801 (2014).
[8] J. Wagemans, C. Wagemans, G. Goeminne, O. Serot, M. Loiselet, and M. Gaelens, Phys. Rev. C, **65**, 034614 (2002).
[9] R. M. Sanders, Physical Review, **104**, 1434 (1956).
[10] P. E. Koehler and S. M. Graff, Phys. Rev. C, **44**, 2788 (1991).
[11] H. Schatz, F. Kaeppeler, P. E. Koehler, M. Wiescher, and H.-P. Trautvetter, Astrophys. J., **413**, 750 (1993).
[12] G. Baur, C. A. Bertulani, and H. Rebel, Nuclear Physics A, **458**, 188 (1986).
[13] S. Cherubini, V. N. Kondratyev, M. Lattuada, C. Spitaleri, D. Miljanic, M. Zadro, and G. Baur, Astrophys. J., **457**, 855 (1996).
[14] C. Spitaleri, M. Aliotta, S. Cherubini, M. Lattuada, D. Miljanić , S. Romano, N. Soic, M. Zadro, and R. A. Zappalà, Phys. Rev. C, **60**, 055802 (1999).
[15] C. Spitaleri, L. Lamia, A. Tumino, R. G. Pizzone, S. Cherubini, A. del Zoppo, P. Figuera, M. La Cognata, A. Musumarra, M. G. Pellegriti, A. Rinollo, C. Rolfs, S. Romano, and S. Tudisco, Phys. Rev. C, **69**, 055806 (2004).
[16] C. Spitaleri, A. M. Mukhamedzhanov, L. D. Blokhintsev, M. L. Cognata, R. G. Pizzone, and A. Tumino, Physics of Atomic Nuclei, **74**, 1725 (2011).
[17] M. Gulino, C. Spitaleri, X. D. Tang, G. L. Guardo, L. Lamia, S. Cherubini, B. Bucher, V. Burjan, M. Couder, P. Davies, R. deBoer, X. Fang, V. Z. Goldberg, Z. Hons, V. Kroha, L. Lamm, M. La Cognata, C. Li, C. Ma, J. Mrazek, A. M. Mukhamedzhanov, M. Notani, S. O'Brien, R. G. Pizzone, G. G. Rapisarda, D. Roberson, M. L. Sergi, W. Tan, I. J. Thompson, and M. Wiescher, Physics Review C, **87**, 012801 (2013).
[18] C. E. Rolfs and W. S. Rodney, *Research supported by NSF, Georgetown University, DFG, et al. Chicago, IL, University of Chicago Press, 1988, 579 p.* (1988).
[19] H. J. Assenbaum, K. Langanke, and C. Rolfs, Zeitschrift fur Physik A Hadrons and Nuclei, **327**, 461 (1987).
[20] F. Strieder, C. Rolfs, C. Spitaleri, and P. Corvisiero, Naturwissenschaften, **88**, 461 (2001).
[21] A. Tumino, C. Spitaleri, A. Mukhamedzhanov, G. G. Rapisarda, S. Cherubini, V. Crucillá, Z. Elekes, Z. Fülöp, M. Gulino, G. Gyürky, G. Kiss, M. La Cognata, L. Lamia, F. Mudó, R. G. Pizzone, S. Romano, M. L. Sergi, and E. Somorjai, Physical Review Letters, **98**, 252502 (2007).
[22] M. L. Sergi, C. Spitaleri, M. La Cognata, A. Coc, A. Mukhamedzhanov, S. V. Burjan, S. Cherubini, V. Crucillá, M. Gulino, F. Hammache, Z. Hons, B. Irgaziev, G. G. Kiss, V. Kroha, L. Lamia, R. G. Pizzone, S. M. R. Puglia, G. G. Rapisarda, S. Romano, N. de Séréville, E. Somorjai, S. Tudisco, and A. Tumino, Phys. Rev. C, **82**, 032801 (2010).
[23] L. Lamia, C. Spitaleri, V. Burjan, N. Carlin, S. Cherubini, V. Crucillà, M. Gameiro Munhoz, M. Gimenez Del Santo, M. Gulino, Z. Hons, G. G. Kiss, V. Kroha, S. Kubono, M. La Cognata, C. Li, J. Mrazek, A. Mukhamedzhanov, R. G. Pizzone, S. M. R. Puglia, Q. Wen, G. G. Rapisarda, C. Rolfs, S. Romano, M. L. Sergi, E. Somorjai, F. A. Souza, A. Szanto de Toledo, G. Tabacaru, A. Tumino, Y. Wakabayashi, H. Yamaguchi, and S.-H. Zhou, Journal of Physics G Nuclear

Physics, **39**, 015106 (2012).
[24] C. Spitaleri, *Problems of Fundamental Modern Physics*, edited by R. Cherubini, P. Dalpiaz, and B. Minetti (World Scientific, New York, 1991) p. 211.
[25] G. R. Satchler, *Direct Nuclear Reactions, International Series of Monographs on Physics* (Oxford University Press, 1983) p. 211.
[26] I. S. Shapiro, V. M. Kolybasov, and G. R. Augst, Nuclear Physics A, **61**, 353 (1965), ISSN 0029-5582.
[27] I. S. Shapiro, Soviet Physics Uspekhi, **10**, 515 (1968).
[28] I. S. Shapiro, *Interaction of High-Energy Particles with Nuclei*, edited by T. E. O. Ericson (1967) p. 210.
[29] R. E. Tribble, C. A. Bertulani, M. La Cognata, A. M. Mukhamedzhanov, and C. Spitaleri, Reports on Progress in Physics, **77**, 106901 (2014).
[30] M. La Cognata, C. Spitaleri, A. M. Mukhamedzhanov, B. Irgaziev, R. E. Tribble, A. Banu, S. Cherubini, A. Coc, V. Crucillà, V. Z. Goldberg, M. Gulino, G. G. Kiss, L. Lamia, J. Mrazek, R. G. Pizzone, S. M. R. Puglia, G. G. Rapisarda, S. Romano, M. L. Sergi, G. Tabacaru, L. Trache, W. Trzaska, and A. Tumino, Physical Review Letters, **101**, 152501 (2008), arXiv:0806.1274 [nucl-ex].
[31] M. La Cognata, C. Spitaleri, A. Mukhamedzhanov, A. Banu, S. Cherubini, A. Coc, V. Crucillà, V. Goldberg, M. Gulino, B. Irgaziev, G. G. Kiss, L. Lamia, J. Mrazek, R. G. Pizzone, S. M. R. Puglia, G. G. Rapisarda, S. Romano, M. L. Sergi, G. Tabacaru, L. Trache, R. E. Tribble, W. Trzaska, and A. Tumino, Astrophys. J., **708**, 796 (2010).
[32] E. I. Dolinsky, P. O. Dzhamalov, and A. M. Mukhamedzhanov, Nuclear Physics A, **202**, 97 (1973).
[33] A. M. Mukhamedzhanov, L. D. Blokhintsev, B. F. Irgaziev, A. S. Kadyrov, M. La Cognata, C. Spitaleri, and R. E. Tribble, Journal of Physics G Nuclear Physics, **35**, 014016 (2008), arXiv:0708.0658 [nucl-th].
[34] L. Lamia, M. La Cognata, C. Spitaleri, B. Irgaziev, and R. G. Pizzone, Phys. Rev. C, **85**, 025805 (2012).
[35] E. Costanzo, M. Lattuada, S. Romano, D. Vinciguerra, and M. Zadro, Nuclear Instruments and Methods in Physics Research A, **295**, 373 (1990).
[36] D. R. Tilley, H. R. Weller, C. M. Cheves, and R. M. Chasteler, Nuclear Physics A, **595**, 1 (1995).
[37] M. Zadro, D. Miljanić, C. Spitaleri, G. Calvi, M. Lattuada, and F. Riggi, Phys. Rev. C, **40**, 181 (1989).
[38] M. La Cognata, C. Spitaleri, A. Mukhamedzhanov, V. Goldberg, B. Irgaziev, L. Lamia, R. G. Pizzone, M. L. Sergi, and R. E. Tribble, Nuclear Physics A, **834**, 658 (2010).
[39] I. J. Thompson, Comput. Phys. Rep., **7**, 167 (1987).
[40] C. M. Perey and F. G. Perey, Atomic Data and Nuclear Data Tables, **17**, 1 (1976).
[41] R. G. Pizzone, C. Spitaleri, S. Cherubini, M. La Cognata, L. Lamia, D. Miljanic', A. Musumarra, S. Romano, A. Tumino, S. Tudisco, and S. Typel, Phys. Rev. C, **71**, 058801 (2005).
[42] R. G. Pizzone, C. Spitaleri, A. M. Mukhamedzhanov, L. D. Blokhintsev, C. A. Bertulani, B. F. Irgaziev, M. L. Cognata, L. Lamia, and S. Romano, Phys. Rev. C, **80**, 025807 (2009).
[43] A. M. Mukhamedzhanov, M. La Cognata, and V. Kroha, Phys. Rev. C, **83**, 044604 (2011), arXiv:1101.1924 [nucl-ex].
[44] M. La Cognata, C. Spitaleri, O. Trippella, G. G. Kiss, G. V. Rogachev, A. M. Mukhamedzhanov, M. Avila, G. L. Guardo, E. Koshchiy, A. Kuchera, L. Lamia, S. M. R. Puglia, S. Romano, D. Santiago, and R. Spartà, Astrophys. J., **777**, 143 (2013).
[45] A. M. Lane and R. G. Thomas, Reviews of Modern Physics, **30**, 257 (1958).
[46] M. La Cognata, S. Palmerini, C. Spitaleri, I. Indelicato, A. M. Mukhamedzhanov, I. Lombardo, and O. Trippella, Astrophys. J., **805**, 128 (2015).
[47] M. Gai, R. Keddy, D. A. Bromley, J. W. Olness, and E. K. Warburton, Phys. Rev. C, **36**, 1256 (1987).
[48] C. Iliadis, *Nuclear Physics of Stars, by Christian Iliadis. ISBN 978-3-527-40602-9. Published by Wiley-VCH Verlag, Wenheim, Germany, 2007.* (Wiley-VCH Verlag, 2007).